Model Predictive Trajectory Optimization and Control for Autonomous Surface Vessels Considering Traffic Rules

Anastasios Tsolakis, Rudy R. Negenborn, Vasso Reppa, Laura Ferranti

***Abstract*—This paper presents a rule-compliant trajectory optimization method for the guidance and control of Autonomous Surface Vessels. The method builds on Model Predictive Contouring Control and incorporates the International Regulations for Preventing Collisions at Sea relevant to motion planning. We use these rules for traffic situation assessment and to derive traffic-related constraints that are inserted in the optimization problem. Our optimization-based approach enables the formalization of abstract verbal expressions, such as traffic rules, and their incorporation in the trajectory optimization algorithm along with the dynamics and other constraints that dictate the system's evolution over a sufficiently long planning horizon. The ability to plan considering different types of constraints and the system's dynamics, over a long horizon in a unified manner, leads to a proactive motion planner that mimics rule-compliant maneuvering behavior, suitable for navigation in mixed-traffic environments. The efficacy and scalability of the derived algorithm are validated in different simulation scenarios, including complex traffic situations with multiple Obstacle Vessels.**

***Index Terms*—Autonomous Surface Vessels, Model Predictive Control, Traffic Regulations**

I. Introduction

OVER the past decade, we have witnessed the world of transportation rapidly advancing towards an increased level of automation. While the automotive industry has had the leading role in this trend, the maritime sector is also progressing towards developing and utilizing autonomous maritime systems in many applications including transportation [1], large-scale monitoring [2] or search and rescue missions [3]. Among the main societal benefits, the most interesting ones concern greater efficiency, reduced operational costs, and increased safety. According to [4], over the period 2014-2020, accidents of navigational nature (collisions, contacts, and groundings/strandings) represented almost 43% of all occurrences while human actions accounted for almost 61% of the contributing factors. Therefore, autonomous maritime navigation has the potential to significantly reduce the risk of collisions, which often lead to human casualties, damaged property, and devastating environmental disasters.

Despite the numerous benefits that autonomy has to offer in the maritime industry, the deployment of Autonomous Surface Vessels (ASVs) in real traffic environments is still limited. One of the main challenges to address relates to the transition period in which ASVs will be expected to co-exist with human-operated vessels in dense traffic environments, such as ports and inland waterways. This raises major societal concerns about the capabilities of the ASVs to interact safely with human-operated vessels in mixed-traffic conditions without causing disruptions or jeopardizing human safety. In this work, we propose a rule-compliant trajectory optimization and control method for ASVs that allows navigation in mixed-traffic environments.

Safety in autonomous maritime navigation is a broad and active topic (refer to [5] for an overview). Ongoing research regarding safety has focused on the problem of interpretation and incorporation of the International Regulations for Preventing Collisions at Sea (COLREGs) [6] in autonomous navigation. Fuzzy logic [7], Dynamic Bayesian Networks (DBN) [8, 9] as well as Finite-State Machines (FSM) [10] have been proposed for situational awareness and decision making. For the task of collision avoidance, methods of subsets of controls, such Velocity Obstacles (VO) [11, 12] and some extensions like Generalized Velocity Obstacles (GVO) [13], Probabilistic Velocity Obstacles (PVO) [14], Dynamic Reciprocal Velocity Obstacles (DRVO) [15] or Optimal Reciprocal Collision Avoidance (ORCA) [16] as well as methods of physical analogies, such as Artificial Potential Fields (APF) [17–19] have been studied thoroughly to work along with COLREGs, as they are methods of low computational complexity. This simplicity, however, comes at the cost of being more reactive and difficult to combine with the full set of traffic regulations which may require longer planning horizons. Moreover, these methods usually give a rough direction of where the ASV should move while disregarding vessel dynamics unless additional reachability approximations are used [15].

To plan over longer horizons, search-based methods like A* [20–22], Voronoi Diagrams [23], and optimal Rapidly-exploring Random Trees (RRT*) [24, 25] have also been employed. They search for a dynamically feasible path in a joint time-state space by either creating artificial costs or obstacles in the discrete grid map to resemble rule-compliant maneuvers. Because the trajectories are computed in the configuration space, they are often non-smooth and their computation is expensive. Moreover, these methods are hard to combine with the complete set of traffic regulations and may even ignore some of the rules in multi-vessel situations [24]. Recently, learning-based methods have also been investigated in con-

This work has been partially supported by the Dutch Science Foundation NWO-TTW within the Veni project HARMONIA (nr. 18165) and the Researchlab Autonomous Shipping (RAS) at TU Delft.

The authors are with the departments of Cognitive Robotics (CoR) and Maritime and Transport Technology (MTT), Delft University of Technology, 2628 CD Delft, The Netherlands (e-mail: a.tsolakis@tudelft.nl). The authors would like to thank the Autonomous Multi-Robots lab (TU Delft) for sharing the code for MPCC used as a building block for our approach.

junction with the traffic rules [26, 27], though drawbacks in these methods often include poor generalizability, convergence to local minima, and lack of formal guarantees.

A popular category for motion planning under COLREGs includes optimization-based methods. Our method fits in this category as well. The main benefit of these methods is the potential to combine multiple objectives and constraints of different nature in a single control module. Among the limitations, the most important ones include deadlocks (due to the local nature of the computed path) and high computational demands (depending on the complexity of the formulated problem). To circumvent these limitations, [28] established a sample-based Model Predictive Control (MPC) approach that considers a finite space of control inputs. Unlike typical MPC formulations, these methods do not identify the best action at every time step during trajectory generation. This work was tested with extensive field verification [29, 30] and it was further extended in other research directions such as Scenario-Based MPC [31, 32]. In [33], the task of navigation under COLREGs is expressed as a multi-objective optimization problem where a particle swarm optimization algorithm is used for its solution. While these methods are suitable in cases of limited computation capacity, they are not guaranteed to converge, and thus, a collision-free path may not be found.

Optimization-based algorithms that rely on conventional gradient-based methods have been studied as well [34–37] having the benefit of exploring the entire control input space. However, all aforementioned approaches rely on a heuristic cost function for rule compliance (that either combines hazard metrics or creates repulsive fields based on the geometrical situation). The use of soft constraints for safety-critical tasks such as rule compliance is questionable since there can be conflicts with other mission objectives (e.g., trajectory tracking). Works in which rule compliance is enforced by introducing hard state constraints to the optimization problem include [38, 39]. In [38] however, the designed constraint is too conservative as it restricts the heading of the ASV and it does not take advantage of state predictions. In [39], hard constraints based on a half-space definition for the domain of the encountered vessels are defined based on their relative position with respect to the ASV and a deflection angle as a parameter. However, that particular definition can lead to infeasibilities since the position of the ASV is not taken into account while tuning this parameter. Moreover, the resulting constraints are nonlinear which may complicate the solution of the optimization problem.

In this work we extend the idea originally presented in [40] where we approached the problem of navigation in mixed-traffic environments by introducing a trajectory optimization algorithm for computing safe and rule-compliant trajectories for ASVs based on Model Predictive Contouring Control (MPCC) since the latter has been proven to be especially suitable for autonomous vehicle applications [37, 40–44]. In contrast to other works that rely on heuristic hazard metrics and soft constraints for rule compliance, we rely on a purely geometric interpretation of the relevant rules and formulate hard constraints to enforce rule-compliant maneuvers while the vessel follows a time-invariant reference path. We formulate these constraints as affine expressions to keep the structure of the optimization problem simple and the algorithm scalable with respect to the number of Obstacle Vessels (OVs). While the collision-free space is generally nonconvex [45], the specific design of our constraints establishes a convex search space, encompassing homotopy-equivalent trajectories. Moreover, we leverage the predictive nature of the controller resulting in proactive, less conservative actions for the ASV while respecting the relevant traffic rules. Last but not least, we have also extended our work with respect to [40] by considering the dynamic model of the vessel including input and state constraints. The result is a trajectory optimization algorithm that achieves path following by generating dynamically feasible, rule-compliant, collision-avoiding trajectories within the prediction horizon while respecting actuator limitations as well. The contributions of this work are:

- A formal derivation of affine constraints that guarantees rule compliance in a convex search space.
- Simplified transition expressions in the traffic rule decision-making module that rely on the design of the affine constraints.
- An algorithm that scales to multiple obstacles and allows the vessels to safely navigate through dense traffic environments.

Section II describes the trajectory optimization problem. Section III describes the vessel dynamics and Section IV the path-following task. Decision-making based on the traffic rules is studied in Section V and the rule constraints are formulated in Section VI. Finally, Section VII presents simulation results and Section VIII concludes the paper.

II. Problem Formulation

Consider that the ASV is moving in a planar workspace $\mathcal{W} = \mathbb{R}^2$. The motion is described by the discrete, nonlinear dynamical system:

$$\boldsymbol{z}(t+1) = \boldsymbol{f}(\boldsymbol{z}(t), \boldsymbol{u}(t)), \quad t = 0, 1, \ldots, \tag{1}$$

with state $\boldsymbol{z} \in \mathcal{Z}$ and control input $\boldsymbol{u} \in \mathcal{U}$ known by an appropriate set of sensors. We assume planar motion for n OVs as well, with their state defined as $\boldsymbol{z}^i \in \mathcal{Z}^i$, $i = \{1, \ldots, n\}$, known to sufficient precision within an area around the ASV along with an estimate of its length l^i and width w^i via a suitable perception framework [46, 47]. We take into account the subset of COLREGs rules 1-18 that describes navigation of vessels in *"sight of one another"*. The state of the ASV is constrained by these rules expressed mathematically as a set of state constraints denoted as $\mathcal{Z}^R(\boldsymbol{z}_k, \boldsymbol{z}_k^i)$.

Given the current state $\boldsymbol{z}(t)$, a reference path parameterized by path parameter s initialized at $s(t)$, and a prediction of each OV's state $\boldsymbol{z}_{1:N}^i$, we formulate a discrete-time, constrained, receding horizon problem over a finite time horizon N with

the set of states $\boldsymbol{z}_{1:N} \in \mathcal{Z}$, set of inputs $\boldsymbol{u}_{2:N} \in \mathcal{U}$, and set of path parameters $s_{1:N}$ as decision variables:

$$\min_{\boldsymbol{z},\boldsymbol{u},s} \sum_{k=1}^{N-1} J(\boldsymbol{z}_k, \boldsymbol{u}_k, s_k) + J_N(\boldsymbol{z}_N, s_N) \tag{2a}$$

$$\text{s.t.: } \boldsymbol{z}_{k+1} = \boldsymbol{f}(\boldsymbol{z}_k, \boldsymbol{u}_k), \quad k = 1, \dots, N \tag{2b}$$

$$s_{k+1} = g(\boldsymbol{z}_k, s_k), \quad k = 1, \dots, N \tag{2c}$$

$$\boldsymbol{z}_k \in \mathcal{Z} \cap \mathcal{Z}^R(\boldsymbol{z}_k, \boldsymbol{z}_k^i), \quad k = 1, \dots, N \tag{2d}$$

$$\boldsymbol{u}_k \in \mathcal{U}, \quad k = 2, \dots, N \tag{2e}$$

$$\boldsymbol{z}_1 = \boldsymbol{z}(t), \quad s_1 = s(t), \tag{2f}$$

where we denote variables with subscript k as the predicted ones in the receding horizon problem. The solution to the receding horizon problem is the optimal input sequence $\boldsymbol{u}^*_{2:N-1}$ of the ASV that minimizes cost function (2a), under system dynamics (2b), path evolution (2c), state constraints (2d) and input constraints (2e). The cost function (2a) consists of the stage cost that is the sum of the following terms:

$$J(\boldsymbol{z}_k, \boldsymbol{u}_k, s_k) = \underbrace{J_v(\boldsymbol{z}_k) + J_{\boldsymbol{u}}(\boldsymbol{u}_k)}_{\text{dynamic behavior}} + \underbrace{J_e(\boldsymbol{z}_k, s_k) + J_u(\boldsymbol{z}_k)}_{\text{path following}} \tag{3}$$

and the terminal cost $J_N(\boldsymbol{z}_N, s_N)$ that can be designed in order to ensure stability. The first two terms are designed to achieve a desirable dynamic behavior discussed in Section III and the last two for navigation objectives discussed in Section IV. The dynamics (2b) and physical limitations of the state and inputs (2d), (2e) are detailed in Section III and the rule-compliance constraints (2d) that serve the task of rule-compliant collision avoidance are activated according to the decision-making scheme of Section V and are derived in Section VI.

An overview of our COLREGs-compliant navigation architecture is provided in Figure 1. We first encode the traffic rules in an algorithmic framework for situational awareness which is necessary for rule-compliant decision making. The module "Traffic Rule Decision Making" attributes a specific traffic role to the vessels based on which the "Constraint Generation" module generates a set of mathematical constraints that are suitable for a receding horizon problem and can guarantee a rule-compliant motion. The "Trajectory Optimizer" module then computes the trajectory for the vessel while considering the aforementioned constraints and outputs the corresponding control command to the ASV. Alternatively to previous works on MPCC [37, 40–44], we consider dynamic collision avoidance implicitly by enforcing compliance to the traffic rules.

We focus on the subset of the rules that are relevant to motion planning. They can be grouped into three categories: *Traffic Rule Decision Making* (7, 13-18) that analyze the situation and designate a traffic role to each vessel, *Situation Invariant Rules* (6, 8.a, 8.d) that apply irrespective of the traffic situation, and *Situation Dependent Rules* (8.b, 8.c, 8.e, 13-17) that vary according to the traffic role. The rest of the rules are either not implementable in motion planning (rules 1-5, 11, and 12) or can be better included in a higher-level motion planner that generates the reference path to be followed (rules 9 and 10).

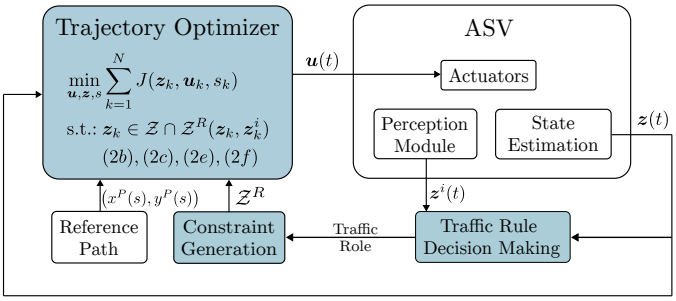

Fig. 1. Schematic method overview (light blue blocks). Given the measured states $\boldsymbol{z}(t)$ and $\boldsymbol{z}^i(t)$, we first infer the traffic role of the vessels based on which a suitable set of constraints is generated. The latter is then inserted in the optimization problem and the first step of the optimal input sequence, $\boldsymbol{u}_1^*$, is applied to the ASV at each control cycle as $\boldsymbol{u}(t)$.

III. Model Dynamics and Physical Limitations

For modeling vessel dynamics we rely on the maneuvering model described in [48]. The ASV's configuration is described by its position $\boldsymbol{p} = (x, y)^\top$, orientation ψ, longitudinal and lateral velocities u, v, and yaw rate r. Note that the velocities are expressed in the body reference frame of the vessel. We then denote as $\boldsymbol{z} = (x, y, \psi, u, v, r)^\top \in \mathcal{Z} \subset \mathbb{R}^6$ the system's state and as $\boldsymbol{u} = (\tau_l, \tau_r, \tau_b, \alpha_l, \alpha_r)^\top \in \mathcal{U} \subset \mathbb{R}^5$ the control input of an ASV with two azimuth thrusters at its beam and one bow thruster. Specifically, we denote as τ_l, τ_r, and α_l, α_r the thrusts and azimuths of the left and right azimuth thruster respectively, and as τ_b the thrust produced by a bow thruster of the ASV. Assuming that there are not any ocean currents, and wind or wave disturbances, the evolution of the system's state is expressed by the following continuous, nonlinear system:

$$\dot{\boldsymbol{z}} = \begin{bmatrix} \boldsymbol{0}_{3\times3} & \boldsymbol{R}(\boldsymbol{z}) \\ \boldsymbol{0}_{3\times3} & -\boldsymbol{M}^{-1}(\boldsymbol{C}(\boldsymbol{z}) + \boldsymbol{D}(\boldsymbol{z})) \end{bmatrix} \boldsymbol{z} + \begin{bmatrix} \boldsymbol{0}_{3\times3} \\ \boldsymbol{M}^{-1} \end{bmatrix} \boldsymbol{\tau}(\boldsymbol{u}), \tag{4a}$$

with:

$$\boldsymbol{M} = \boldsymbol{M_{RB}} + \boldsymbol{M_A}, \tag{4b}$$

$$\boldsymbol{C}(\boldsymbol{z}) = \boldsymbol{C_{RB}}(\boldsymbol{z}) + \boldsymbol{C_A}(\boldsymbol{z}), \tag{4c}$$

$$\boldsymbol{D}(\boldsymbol{z}) = \boldsymbol{D_L} + \boldsymbol{D_{NL}}(\boldsymbol{z}), \tag{4d}$$

$$\boldsymbol{\tau} = \begin{pmatrix} \tau_l \cos\alpha_l + \tau_r \cos\alpha_r \\ \tau_l \sin\alpha_l + \tau_r \sin\alpha_r + \tau_b \\ w_{lr}(\tau_r \cos\alpha_r - \tau_l \cos\alpha_l) - \\ \quad l_{lr}(\tau_l \sin\alpha_l - \tau_r \cos\alpha_r) + l_b\tau_b \end{pmatrix} \tag{4e}$$

where $\boldsymbol{R}(\boldsymbol{z})$ is the rotation matrix, $\boldsymbol{M_{RB}}$ the rigid-body mass matrix, $\boldsymbol{C_{RB}}(\boldsymbol{z})$ the rigid-body Coriolis and centripetal matrix, $\boldsymbol{M_A}$ the added-mass matrix, $\boldsymbol{C_A}(\boldsymbol{z})$ the added Coriolis and centripetal matrix, $\boldsymbol{D_L}$, $\boldsymbol{D_{NL}}(\boldsymbol{z})$, the linear and nonlinear damping matrices, $\boldsymbol{\tau}$ the generalized force vector acting on the vessel, and w_{lr}, l_{lr}, l_b are length parameters that describe the configuration of the thrusters. The added-mass and Coriolis matrices are introduced due to hydrodynamic forces when we consider the additional forces resulting from the fluid acting on the vessel. The continuous system dynamics (4) are discretized

with a Runge-Kutta method in the form (2b) to solve the receding horizon problem (2).

We also consider actuator limitations $\tau_l \in [\tau_{l_{\min}}, \tau_{l_{\max}}]$, $\tau_r \in [\tau_{r_{\min}}, \tau_{r_{\max}}]$, $\tau_b \in [\tau_{b_{\min}}, \tau_{b_{\max}}]$, $\alpha_l \in [\alpha_{l_{\min}}, \alpha_{l_{\max}}]$, $\alpha_r \in [\alpha_{r_{\min}}, \alpha_{r_{\max}}]$, where $\tau_{l_{\min}}$, $\tau_{l_{\max}}$, $\tau_{r_{\min}}$, $\tau_{r_{\max}}$, $\tau_{b_{\min}}$, $\tau_{b_{\max}}$, $\alpha_{l_{\min}}$, $\alpha_{l_{\max}}$, $\alpha_{r_{\min}}$, $\alpha_{r_{\max}}$ are the minimum and maximum control inputs respectively.

We can further include two terms in the objective function to tune the response of the dynamical system. First of all, to reduce undesirable drift of the vessel, we include the term:

$$J_v(\boldsymbol{z}_k) = q_v v_k^2, \quad k = 1, \dots, N, \tag{5}$$

to penalize lateral velocity v with tuning parameter q_v. Moreover, we penalize excessive control input by including the term:

$$J_{\boldsymbol{u}}(\boldsymbol{u}_k) = \boldsymbol{u}_k^\top \boldsymbol{Q}_{\boldsymbol{u}} \boldsymbol{u}_k, \quad k = 1, \dots, N, \tag{6}$$

where

$$\boldsymbol{Q}_{\boldsymbol{u}} = \begin{bmatrix} q_{\tau_l} & 0 & 0 & 0 & 0 \\ 0 & q_{\tau_r} & 0 & 0 & 0 \\ 0 & 0 & q_{\tau_b} & 0 & 0 \\ 0 & 0 & 0 & q_{\alpha_l} & 0 \\ 0 & 0 & 0 & 0 & q_{\alpha_r} \end{bmatrix}, \tag{7}$$

is a tuning parameter matrix. The rest of the states are subject to limitations imposed by the traffic rules as discussed in Section VI.

IV. Path Following

The key idea in the MPCC problem formulation as expressed in (2), is that the vehicle does not need to track a reference trajectory but rather a time-invariant reference path via the objective function under certain input and state constraints. For the path following objective, we follow the approach in [41, 43] in which the vessel at time t is at position $\boldsymbol{p}(t) = (x(t), y(t))^\top$ and tracks a continuously differentiable two-dimensional reference path $(x^P(s), y^P(s))$ with path tangential angle $\psi^P(s) = \arctan(\partial y^P(s)/\partial x^P(s))$, parameterized by the arc length s. The arc length s of the closest point to the ASV can be approximated with an evolution of the path parameter (2c) described as:

$$s_{k+1} = s_k + u_k \Delta k, \tag{8}$$

with Δk denoting the prediction timestep, u_k the discretized longitudinal velocity, and s_1 initialized at each planning cycle as the point of the path that is closest to the ASV's position. The path error vector $\boldsymbol{e}_k$ is then defined as:

$$\boldsymbol{e}_k(\boldsymbol{z}_k, s_k) = \begin{bmatrix} \tilde{e}^l(\boldsymbol{z}_k, s_k) \\ \tilde{e}^c(\boldsymbol{z}_k, s_k) \end{bmatrix}, \tag{9}$$

where the longitudinal error is defined as:

$$\tilde{e}^l(\boldsymbol{z}_k, s_k) = -\begin{pmatrix} \cos\psi^P(s_k) & \sin\psi^P(s_k) \end{pmatrix} \begin{pmatrix} x_k - x^P(s_k) \\ y_k - y^P(s_k) \end{pmatrix}, \tag{10}$$

and the contouring error as:

$$\tilde{e}^c(\boldsymbol{z}_k, s_k) = \begin{pmatrix} \sin\psi^P(s_k) & -\cos\psi^P(s_k) \end{pmatrix} \begin{pmatrix} x_k - x^P(s_k) \\ y_k - y^P(s_k) \end{pmatrix}, \tag{11}$$

To achieve path tracking using the definition of the error defined in (9), one of the cost terms in the objective function (2a) will take the form:

$$J_e(\boldsymbol{z}_k, s_k) = \boldsymbol{e}_k^\top \boldsymbol{Q}_{\boldsymbol{e}} \boldsymbol{e}_k, \quad k = 1, \dots, N, \tag{12}$$

where

$$\boldsymbol{Q}_{\boldsymbol{e}} = \begin{bmatrix} q_{e_l} & 0 \\ 0 & q_{e_c} \end{bmatrix}, \tag{13}$$

is a tuning parameter matrix that penalizes deviation from the reference path.

To progress along the path, the ASV needs to have a non-zero longitudinal velocity u_k. This can be achieved by another term in the objective function:

$$J_u(\boldsymbol{z}_k) = q_u(u_k - u_{\text{ref}})^2, \quad k = 1, \dots, N, \tag{14}$$

where u_{ref} denotes a desired reference speed and q_u is a weighting factor to penalize deviation from the reference speed. Thus, the vessel can track a time-invariant path, the progress upon which is determined by the predicted longitudinal speed u_k. In this manner, the path-following task is quite flexible and allows the vessel to deviate from it if necessary (e.g., for collision avoidance) without creating conflicting objectives. The choice of these parameters q_u, u_{ref} is further discussed in Section VI as it plays a role in rule compliance as well. For a more detailed description of the path following task the reader is referred to [41, 43].

V. Traffic Rule Decision Making

Situation analysis and classification refers to a decision-making scheme that attributes a pairwise traffic role to the ASV and each OV, based on a subset of the traffic rules. This topic has been studied in great detail in [14, 35] among other works and is of great importance as it dictates the actions each vessel needs to follow in order to avoid collision in a safe manner. This section presents the simple Finite-State Machine (FSM) presented in Figure 2 that provides a pairwise role symmetry with transitions that consider properly defined entry and exit criteria for each state. The FSM has three states that represent the traffic role of the vessel - *Stand On* (SO), *Give Way* (GW), or *Emergency* (EM) as discussed in this Section. The corresponding transition expressions to enter or exit each state of the FSM namely, $T_{\text{GW}}^{\text{ent}}$, $T_{\text{GW}}^{\text{ext}}$, $T_{\text{EM}}^{\text{ent}}$, and $T_{\text{EM}}^{\text{ext}}$, depend on the current states $\boldsymbol{z}(t)$ and $\boldsymbol{z}^i(t)$ of the ASV and each OV and their derivation is presented step-by-step in this Section.

The first step is to identify if there exists risk of collision with an OV within the vicinity of the ASV. Rule 7 considers *"Risk of Collision"* with part 7.d.i describing that *"such risk shall be deemed to exist if the compass bearing of an approaching vessel does not appreciably change"* and part 7.d.ii *"such risk may sometimes exist even when an appreciable bearing change is evident, particularly when approaching a very large vessel or a tow or when approaching a vessel at close range"*. According to Rule 17.a.i, *"Where one of two vessels is to keep out of the way the other shall keep her course and speed"*. Thus, we can assume that any vessel encountered within an encounter radius denoted as ρ_{enc} around the ASV would keep a constant velocity if there is no risk of collision.

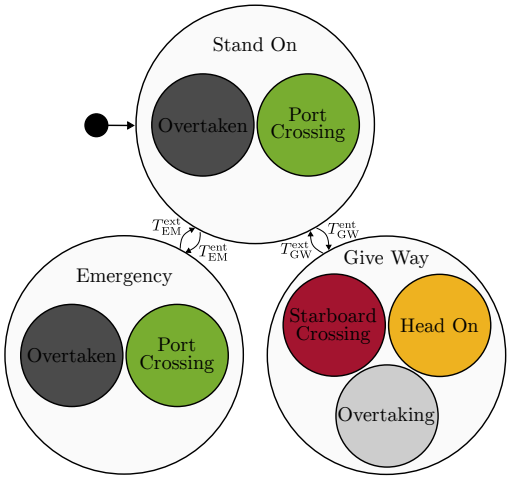

Fig. 2. Schematic representation of the FSM for traffic role decision making. Traffic situations that lead to the same traffic role are grouped for simplicity.

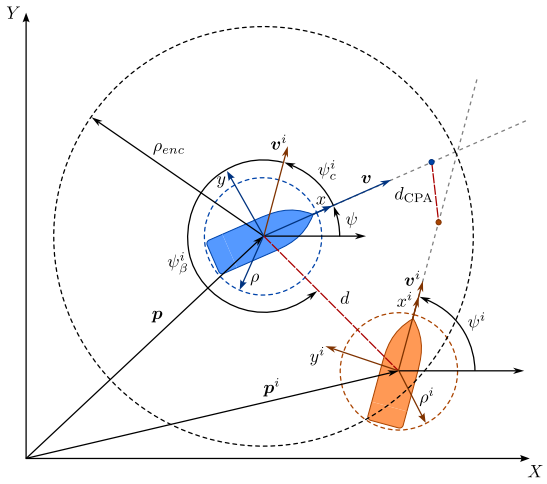

Fig. 3. Encounter situation analysis between the ASV and OV i. Their current states $\boldsymbol{z}(t)$ and $\boldsymbol{z}^i(t)$ are used to determine the distance at the Closest Point of Approach (d_{CPA}) and thus if risk of collision exists assuming constant velocities.

We can then integrate the position vector equations from the current time t until some time in the future denoted as τ:

$$\boldsymbol{p}(\tau) = \boldsymbol{p}(t) + (\tau - t)\tilde{\boldsymbol{R}}(\boldsymbol{z}(t))\boldsymbol{v}(t), \tag{15a}$$

$$\boldsymbol{p}^i(\tau) = \boldsymbol{p}^i(t) + (\tau - t)\tilde{\boldsymbol{R}}(\boldsymbol{z}^i(t))\boldsymbol{v}^i(t), \tag{15b}$$

where we denote as $\boldsymbol{v} = (u, v)^\top$, $\boldsymbol{v}^i = (u^i, v^i)^\top$the translational velocities of the two vessels and as $\tilde{\boldsymbol{R}}(\boldsymbol{z}(t))$ the 2×2 sub-matrix of $\boldsymbol{R}(\boldsymbol{z}(t))$, that maps the translational velocities from each body reference frame to the global reference frame. The current distance between the two vessels is:

$$d(t) = \left\|\boldsymbol{p}(t) - \boldsymbol{p}^i(t)\right\|_2 \tag{16}$$

The distance between two vessels at a future time τ computed at time t, can be expressed as:

$$d(\tau|t) = \left\|\boldsymbol{p}(t) - \boldsymbol{p}^i(t) + (\tau - t)(\tilde{\boldsymbol{R}}(\boldsymbol{z}(t))\boldsymbol{v}(t) - \tilde{\boldsymbol{R}}(\boldsymbol{z}^i(t))\boldsymbol{v}^i(t))\right\|_2 \tag{17}$$

Both $d(t)$ and $d(\tau|t)$ are shown in Figure 3. Finding the minimum of $d(\tau|t)$ is equivalent to finding the minimum of its square, which is a quadratic function with respect to time τ. The minimum of this function is then the solution of $\partial d(\tau|t)^2/\partial\tau = 0$ which results to:

$$t_{\text{CPA}}(t) = -\frac{(\tilde{\boldsymbol{R}}(\boldsymbol{z}(t))\boldsymbol{v}(t) - \tilde{\boldsymbol{R}}(\boldsymbol{z}^i(t))\boldsymbol{v}^i(t))^\top(\boldsymbol{p}(t) - \boldsymbol{p}^i(t))}{\left\|\tilde{\boldsymbol{R}}(\boldsymbol{z}(t))\boldsymbol{v}(t) - \tilde{\boldsymbol{R}}(\boldsymbol{z}^i(t))\boldsymbol{v}^i(t)\right\|_2^2} \tag{18}$$

This future time is known as the time to the *"Closest Point of Approach"*. The corresponding distance is then:

$$d_{\text{CPA}}(t) = \begin{cases} \left\|\boldsymbol{p} - \boldsymbol{p}^i + (\tilde{\boldsymbol{R}}(\boldsymbol{z})\boldsymbol{v} - \tilde{\boldsymbol{R}}(\boldsymbol{z}^i)\boldsymbol{v}^i)t_{\text{CPA}}\right\|_2 & t_{\text{CPA}} \geq 0 \\ d & t_{\text{CPA}} < 0 \end{cases} \tag{19}$$

since $t_{\text{CPA}} < 0$ means that the two vessels are diverging and thus d_{CPA} is the current distance. Dependence on current time t is omitted for readability. We continue by assuming that a rough estimate of the length l^i and width w^i of the other vessel can be inferred by a visual perception or communication system (e.g., Automatic Identification System (AIS)) and the footprint of vessels to be circles of radii $\rho = \sqrt{(l/2)^2 + (w/2)^2}$ and $\rho^i = \sqrt{(l^i/2)^2 + (w^i/2)^2}$, respectively, for the purposes of this module. Then, we can deem that risk of collision exists when $d_{\text{CPA}} < \rho + \rho^i + \rho_s$ which means that the two vessels will be closer than a safety margin ρ_s that for now is chosen arbitrarily. Note that using d_{CPA} as a metric for risk of collision is similar to the requirement of Rule 7 to monitor the relative bearing over time but easier to evaluate risk of collision considering the dimensions of the two vessels. For the purposes of traffic role decision making we use circular footprints as this serves only as a rough estimate of whether or not risk of collision exists. For collision avoidance we use a more accurate approximation of marine vessels' footprints discussed in Section VI.

If a risk of collision exists, the next step is to decide on the actions to be taken by the vessels involved. According to Rules 13-17, there can be three different, pair-wise traffic situations between the two vessels:

- Head-On / Head-On
- Starboard-Crossing / Port-Crossing
- Overtaking / Overtaken

These traffic situations depend on the relative position of the two vessels encoded in the *relative bearing*:

$$\psi_\beta^i(t) = \arctan\left(\frac{\hat{\boldsymbol{y}}^\top\tilde{\boldsymbol{R}}(\boldsymbol{z}(t))(\boldsymbol{p}^i(t) - \boldsymbol{p}(t))}{\hat{\boldsymbol{x}}^\top\tilde{\boldsymbol{R}}(\boldsymbol{z}(t))(\boldsymbol{p}^i(t) - \boldsymbol{p}(t))}\right), \tag{20}$$

and the *relative course*:

$$\psi_c^i(t) = \psi^i(t) - \psi(t), \tag{21}$$

with $\hat{\boldsymbol{x}}$, $\hat{\boldsymbol{y}}$ denoting the unit vectors of the ASV's body reference frame shown in Figure 3. The combination of $\psi_\beta^i(t)$ and $\psi_c^i(t)$ defines the role classification shown in Figure 4 similar to that found in [14]. To determine the head-on situation, we need to define one additional parameter ψ_h that defines a threshold for the relative course $\psi_c^i(t)$. Unfortunately, it is not clearly stated in the rules what the value should be but according to [35], court decisions indicate $\psi_h = \pm 6°$. Note that for some combinations of $\psi_\beta^i(t)$ and $\psi_c^i(t)$ the traffic

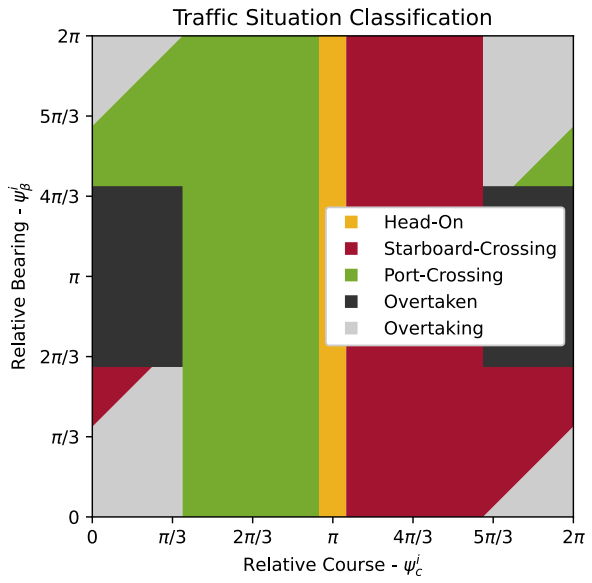

Fig. 4. Traffic situation classification as a function of the relative course ψ_c^i, and the relative bearing ψ_β^i described in [6]. Note that the same figure from the perspective of the OV would be role-symmetric since pairwise-role symmetry is necessary.

situations may not be considered if $d_{\text{CPA}} \geq \rho + \rho^i + \rho_s$ and risk of collision is not deemed to exist.

According to the rules, in each traffic situation, a vessel can be either a *Give-Way* (GW) vessel, which must take collision-avoiding action, or a *Stand-On* (SO) vessel, which is required to maintain its course and speed. According to this classification, each vessel has a GW or SO role as described in Rules 16 and 17 respectively. While Rule 16 is straightforward for the GW vessel, Rule 17.a.ii describes that *"The latter vessel"* (i.e., the SO) *"may however take action to avoid collision by her maneuver alone, as soon as it becomes apparent to her that the vessel required to keep out of the way is not taking appropriate action in compliance with these Rules"* and Rule 17.b states that *"When, from any cause, the vessel required to keep her course and speed finds herself so close that collision cannot be avoided by the action of the give-way vessel alone, she shall take such action as will best aid to avoid collision"*. Thus, another role emerges for the SO vessel which in some cases must take collision-avoiding action. We will denote this state here as *Emergency* (EM) state. This situation is studied in depth in [49] where they design a collision alert system for SO vessels. In summary, the following roles are expected from each vessel:

- GW: Head-On, Overtaking, and Starboard-Crossing
- SO: Port-Crossing and Overtaken with no needed action
- EM: Port-Crossing and Overtaken with emergency action

The last thing to consider for a complete encounter situation analysis is the entry and exit criteria. In [35] thresholds on d_{CPA} and t_{CPA} are defined in order to determine entry and exit criteria. However, these values may change rapidly especially in multi-vessel scenarios while the vessels are still in close proximity and likely to perform more complex maneuvers. Unfortunately, the rules do not describe explicitly for how long these pairwise roles should hold. Nevertheless, Rule 13.d clearly states that *"Any subsequent alteration of the bearing between the two vessels shall not make the overtaking vessel a crossing vessel within the meaning of these Rules or relieve her of the duty of keeping clear of the overtaken vessel until she is finally past and clear"*. Based on that we can infer that the pairwise roles, as long as they are attributed to the vessels, should remain consistent until the encounter situation is over. Thus, we keep the pairwise roles for as long as the other vessel remains within the encounter radius ρ_{enc} of the ASV for a normal traffic situation. An emergency situation is considered when $d < \rho_{\text{emg}}$ where ρ_{emg} defines the radius of a circular area around the ASV within which, if a GW vessel enters, it is inferred it does not comply with the rules. This is then deemed to be an emergency situation for which even as an SO vessel the ASV needs to take action to avoid collision according to Rule 17.

Lastly, in compliance with Rule 18.a, we assume that the perception system used by the ASV (e.g., similar to the one in [47]) can determine if the other vessel is *"(i) a vessel not under command; (ii) a vessel restricted in her ability to maneuver*; (iii) a vessel engaged in fishing; (iv) a sailing vessel." which will set the role of the ASV to GW.

The aforementioned, lead to the design of the FSM illustrated in Figure 2 that is governed by the following Boolean expressions according to [6] that depend on the current states $\boldsymbol{z}(t)$ and $\boldsymbol{z}^i(t)$:

$$T_{\text{enc}} = d(t) < \rho_{\text{enc}} \tag{22a}$$
$$T_{\text{rsk}} = d_{\text{CPA}}(t) < \rho + \rho^i + \rho_s \tag{22b}$$
$$T_{\text{hdn}} = (\psi_c^i(t) \geq \pi - \psi_h) \wedge (\psi_c^i(t) < \pi + \psi_h) \tag{22c}$$
$$T_{\text{str}} = (\psi_c^i(t) \geq \pi + \psi_h) \wedge (\psi_c^i(t) < 13\pi/8) \tag{22d}$$
$$T_{\text{brn}} = (\psi_c^i(t) \geq 13\pi/8) \wedge (\psi_c^i(t) < 3\pi/8) \tag{22e}$$
$$T_{\text{ovr}} = (\pi + \psi_\beta^i(t) - \psi_c^i(t) \geq 5\pi/8) \wedge (\pi + \psi_\beta^i(t) - \psi_c^i(t) < 11\pi/8) \tag{22f}$$
$$T_{\text{stb}} = (\psi_\beta^i(t) \geq 0) \wedge (\psi_\beta^i(t) < 5\pi/8) \tag{22g}$$
$$T_{\text{emg}} = d(t) < \rho_{\text{emg}} \tag{22h}$$

which combined formulate the final transition expressions for the FSM of Figure 2:

$$T_{\text{GW}}^{\text{ent}} = T_{\text{enc}} \wedge \{T_{\text{rsk}} \wedge [T_{\text{hdn}} \vee T_{\text{str}} \vee (T_{\text{brn}} \wedge (T_{\text{ovr}} \vee T_{\text{stb}}))]\} \tag{23a}$$
$$T_{\text{GW}}^{\text{ext}} = \neg T_{\text{enc}} \tag{23b}$$
$$T_{\text{EM}}^{\text{ent}} = T_{\text{emg}} \tag{23c}$$
$$T_{\text{EM}}^{\text{ext}} = \neg T_{\text{emg}}, \tag{23d}$$

In the equations above, logic symbols $\wedge$, $\vee$, $\neg$, stand for "and", "or" and "not" respectively. Note that it is intentional that the EM state can only be reached from the SO state as we would like to allow vessels to come closer than ρ_{emg} if they adhere to the rules and they are assigned a pair of SO-GW roles. The FSM of Figure 2 can then assign the appropriate traffic role to each of the vessels. Note that for simplicity, the Overtaking, Head-On, and Starboard-Crossing situations have been grouped under the GW state and the Overtaken and Port-Crossing situations under the EM state, since the required

actions are the same. Based on the traffic role assigned in this module, the corresponding collision avoidance constraints described in the next sections are generated and inserted in the optimization problem (2) before each planning cycle.

VI. Constraint Generation

A. Situation Invariant Rules

The first rule that is implementable in a local motion planning algorithm is Rule 6, which describes that *"Every vessel shall at all times proceed at a safe speed so that she can take proper and effective action to avoid collision and be stopped within a distance appropriate to the prevailing circumstances and conditions"*. This rule is already implemented as a soft constraint in the cost function (2a) given in (14) as part of the path following task. The vessel's reference speed that needs to be followed can be set according to the local regulations that are applicable in its environment (e.g., open sea, canal, port, etc.) and the type of the vessel.

Rule 8 describes the proper action to avoid collision: Rule 8.a specifically describes that*"Any action to avoid collision [...], made in ample time [...]"*. This requirement is implemented with the already defined encountered distance ρ_{enc} between the two vessels which determines when the ASV has encountered another vessel and needs to assess the situation (see Figure 3).

Rule 8.d describes that action should be taken such that vessels are passing at a safe distance. While this is not explained adequately in the rules, we can think of what would be the best way to approximate the footprint of the OV. Because of the oblong shape that the vessels usually have, the circumscribed rectangle is a good approximation of the vessel's footprint since it is a simple shape but at the same time not very conservative (e.g., as the circumscribed circle would be). We can then implement this safety distance by enlarging the circumscribed rectangle by some margins $(\rho^i_{\text{bm}}, \rho^i_{\text{sn}}, \rho^i_{\text{pt}}, \rho^i_{\text{sb}})$ depending on the side of the vessel illustrated as the orange dashed rectangle in Figure 5. Since the decision variables include the center of the ASV where the body reference frame is attached, a common practice for the task of collision avoidance is to inflate the footprint of the obstacle by the dimensions of the ASV by using the Minkowski sum [50]. In general, the Minkowski sum depends on the relative orientation as well, which makes the computation of the inflated obstacle's footprint more involved, and the resulting shapes to vary. A simpler way is to approximate the footprint of the ASV with the circumscribed circle which will make the Minkowski sum rotation-invariant. The Minkowski sum of the rectangular bound of vessel i and the circumscribed circle of the ASV with radius ρ is then the rounded orange rectangle illustrated in Figure 5, the most outer "boundary" around the OV. Notice that as done in previous works on MPCC [41–43], the footprint of the ego-vehicle (here the ASV) can be approximated with a multiplicity of offseted circles along the symmetry axis that will make the approximation much less conservative but still favorable in terms of computational complexity. This approximation of the OV's footprint with the safety margins is utilized in the following section where we generate the rule-compliant constraints.

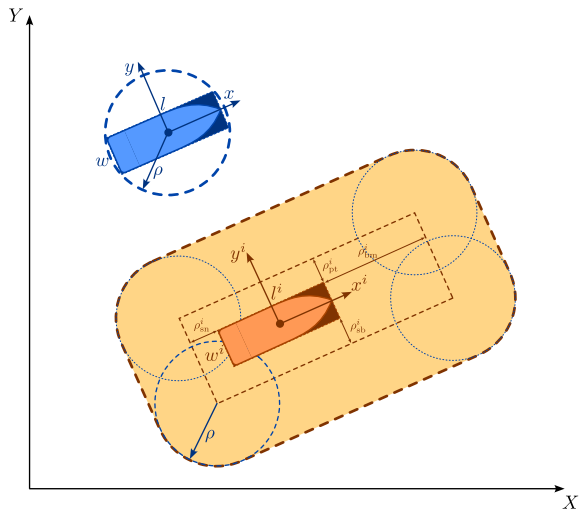

Fig. 5. Footprints of the two vessels for collision avoidance. A rectangle shape is a simple representation of the real footprint of a vessel without being too conservative. The rectangle's sides can be augmented to allow for some safety margin as well. The rectangle is inflated by the radius of the circumscribed circle of the ASV leading to a rounded rectangle. Note that the ability to approximate the ASV with multiple circles of smaller radius can allow for less conservative approximations if needed (e.g. in inland waterways).

B. Situation Dependent Rules

This section discusses rules that hold according to the encounter situation of the ASV. Rule 8.b states that *"Any alteration of course and/or speed to avoid collision shall, [...], be large enough to be readily apparent to another vessel [...]"*. This rule is often ignored leading to vessel maneuvers that are jittery and do not resemble rule-compliant maneuvers. One way to implement this rule is to impose constraints on the angular acceleration $\dot{r}$ and the longitudinal acceleration $\dot{u}$ to be larger than a certain value. However, as explained in [35], this can result in a highly non-convex (and even non-connected) search space and, consequently, in a hard-to-solve nonlinear optimization problem. Moreover, these variables are not included in (2). To circumvent these problems, we consider this rule in the design of constraints for Rules 13-17 later in this section. These constraints will cause the ASV to alter its course in a sufficient, rule compliant manner.

Rule 8.c states that *"If there is sufficient sea-room, alteration of course alone may be the most effective action to avoid a close-quarters situation [...]"*. This is already considered in (14) where we can tune weight q_u accordingly to track the reference speed. According to Rule 8.e, though, the vessel *"[...] shall slacken her speed or take all way off by stopping or reversing her means of propulsion"*. This means that the objective described in term (14) might interfere with collision avoidance as it then describes two conflicting goals for the trajectory optimizer. The problem can be overcome by switching the value of the tuning parameter q_u of cost term (14) according to the vessel role as $q_u \in \{q_{u_{\text{SO}}}, q_{u_{\text{GW}}}, q_{u_{\text{EM}}}\}$ with $q_{u_{\text{EM}}} \ll q_{u_{\text{GW}}} = q_{u_{\text{SO}}}$. Thus, in an emergency situation, the reference velocity following task is relaxed to allow the ASV to slow down or even reverse if necessary.

Next, we consider Rules 13-15, which describe the maneuver a GW vessel should follow in the *Overtaking*, *Head-*

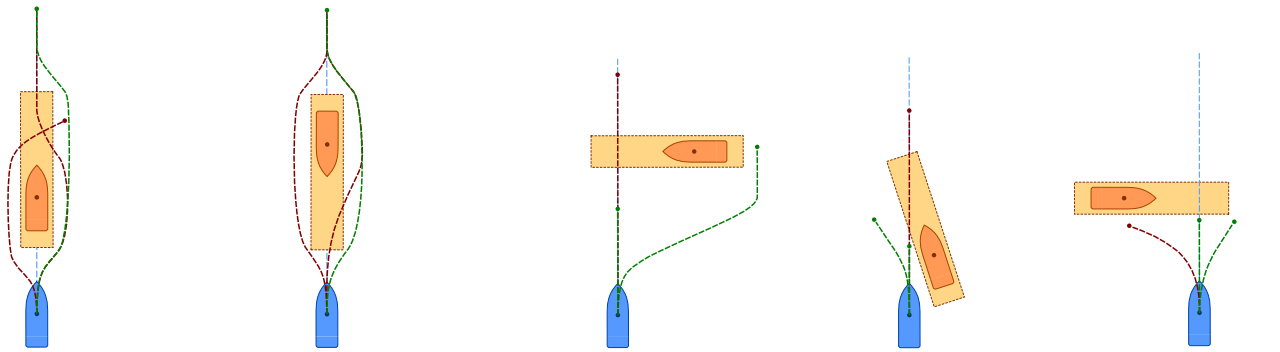

Fig. 6. Rule-compliant (green) and prohibited (red) trajectories for the ASV (blue) in each traffic situation with an OV (orange) according to rules 13-17: The three situations on the left - a) Overtaking, b) Head On , c) Starboard Crossing - are situations where the ASV has a GW role while the two on the right - d) Overtaken, e) Port Crossing - describe suitable emergency maneuvers with the ASV in an EM role.

On, *Starboard Crossing* situations, respectively, as well as Rule 17 which describes emergency actions that arise in the *Overtaken* and *Port Crossing* situations for an EM vessel. Figure 6 presents examples of compliant (green) and non-compliant (red) maneuvers for each situation. In the following, we design suitable constraints to enforce compliant maneuvers while avoiding non-compliant ones.

In most MPC-based works these constraints are implemented as soft constraints via a heuristic cost function that relies on some hazard metric or aims at creating a repulsive field [28–36]. In this work, instead, the goal is to implement these rules as geometric, hard constraints to guarantee a rule-compliant behavior and decouple this task from the tasks of path-following and velocity-following described in the objective function. The design of these constraints should not cause problems with feasibility and allow the solution of (2) in real time. Thus, we design a set of affine constraints for each pairwise situation. Then, in multi-vessel encounters, this will result to a convex polytope around the ASV, a rule-compliant search space in the receding horizon problem (2). We can then have strict rule-compliance guarantees in multi-vessel situations without complicating the solution of the optimization problem. These constraints might be more conservative than other types (e.g., quadratic constraints used in [41, 43]), but they are more suitable to represent the traffic rules as discussed in this Section. To design these constraints, we rely on the notion of the *separating* and *supporting* planes from convex optimization [51].

For each timestep $k \in 1,\dots,N$ along the prediction horizon, a supporting hyperplane of each circle $j \in [1,4]$ with radius ρ centered at the vertices of the inflated rectangle (see Figure 7) of OV $i \in 1,\dots,n$ can be defined as:

$$\mathcal{H}_d^{i,j} : \boldsymbol{d}_k^{i,j} \boldsymbol{p}_k \leq {\boldsymbol{d}_k^{i,j}}^\top \left(\boldsymbol{p}_k^{i,j} + \boldsymbol{d}_k^{i,j} \rho \right), \tag{24}$$

where:

$$\boldsymbol{d}_k^{i,j} = \frac{\left(\hat{\boldsymbol{p}}_k - \boldsymbol{p}_k^{i,j} \right)^\top}{\left\| \hat{\boldsymbol{p}}_k - \boldsymbol{p}_k^{i,j} \right\|}, \tag{25}$$

is the normalized relative position vector defined with $\hat{\boldsymbol{p}}_k$ and $\boldsymbol{p}_k^{i,j}$ the predictions of the ASV and the OV's vertices respectively. For the OV we rely on a constant velocity assumption to derive the predicted positions as:

$$\boldsymbol{p}_k^i = \boldsymbol{p}^i(t) + k \cdot \Delta k \cdot \tilde{\boldsymbol{R}}(\boldsymbol{z}(t)) \boldsymbol{v}^i(t), \tag{26}$$

by inferring its current position $\boldsymbol{p}^i(t)$ and velocity $\boldsymbol{v}^i(t)$. The predicted positions of the vertices are then:

$$\boldsymbol{p}_k^{i,1} = \boldsymbol{p}_k^i + \tilde{\boldsymbol{R}}(\boldsymbol{z}(t)) \begin{pmatrix} (l^i/2 + \rho_{\text{bm}}) \\ (w^i/2 + \rho_{\text{pt}}) \end{pmatrix} \tag{27a}$$

$$\boldsymbol{p}_k^{i,2} = \boldsymbol{p}_k^i + \tilde{\boldsymbol{R}}(\boldsymbol{z}(t)) \begin{pmatrix} (l^i/2 + \rho_{\text{bm}}) \\ -(w^i/2 + \rho_{\text{sb}}) \end{pmatrix} \tag{27b}$$

$$\boldsymbol{p}_k^{i,3} = \boldsymbol{p}_k^i + \tilde{\boldsymbol{R}}(\boldsymbol{z}(t)) \begin{pmatrix} -(l^i/2 + \rho_{\text{st}}) \\ -(w^i/2 + \rho_{\text{sb}}) \end{pmatrix} \tag{27c}$$

$$\boldsymbol{p}_k^{i,4} = \boldsymbol{p}_k^i + \tilde{\boldsymbol{R}}(\boldsymbol{z}(t)) \begin{pmatrix} -(l^i/2 + \rho_{\text{sn}}) \\ (w^i/2 + \rho_{\text{pt}}) \end{pmatrix} \tag{27d}$$

More general predictions from prediction modules can be accommodated as well. For the predictions of the ASV, we employ the trajectory of the previous planning cycle by shifting the previous plan one step forward: $\hat{\boldsymbol{p}}_k \triangleq \hat{\boldsymbol{p}}_{t|k} = \boldsymbol{p}_{t-1|k+1}$ for $k = 1,\dots,N-1$ while for the last step $k = N$ the predicted position is approximated as the linear extrapolation of the last two steps of the previous planning cycle: $\hat{\boldsymbol{p}}_N \triangleq \hat{\boldsymbol{p}}_{t|N} = 2\boldsymbol{p}_{t-1|N} - \boldsymbol{p}_{t-1|N-1}$. Note that the hyperplane of (24) can always be defined as long as $\hat{\boldsymbol{p}}_k \neq \boldsymbol{p}_k^{i,j}$ and is at the same time a separating hyperplane with respect to the ASV which is now reduced to a sequence of single points $\hat{\boldsymbol{p}}_{1:N}$ along the prediction horizon. Hyperplane $\mathcal{H}_d^{i,j}$, illustrated in Figure 7, can be used as a constraint to ensure that the footprints of the ASV and the OV will not overlap thus achieving collision avoidance. However, it cannot enforce rule-compliant trajectories similar to the green ones illustrated in Figure 6. For this reason, we want to rotate this hyperplane in a proper manner and force the generated trajectories as close to the desired ones as possible. That is, to the starboard side of the ASV and behind the OV as implicitly required by Rules 13-17. The range of rotation that keeps the supporting plane of each circle j to be a separating plane with respect to the ASV

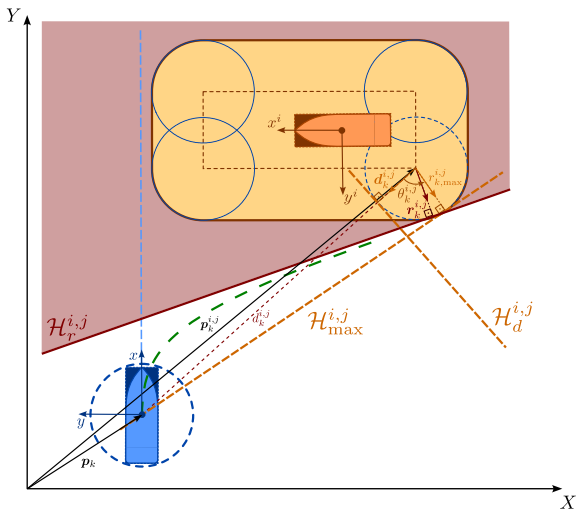

Fig. 7. The affine constraint in the example of a starboard-crossing situation. The constraint restricts the allowable space for the ASV and forces the trajectory away from the reference path and behind the OV for the task of rule-compliant collision avoidance according to the rules.

(each point $\hat{\boldsymbol{p}}_k$) is that between the two orange hyperplanes illustrated in Figure 7 denoted as $\mathcal{H}_d^{i,j}$ and $\mathcal{H}_{\max}^{i,j}$. We are interested in the maximum counter-clockwise rotation of the orange hyperplane $\mathcal{H}_d^{i,j}$ with normal vector $\boldsymbol{d}_k^{i,j}$ that would lead to $\mathcal{H}_{\max}^{i,j}$. The maximum angle of rotation $\theta_k^{i,j}$ is:

$$\theta_k^{i,j} = \begin{cases} \arccos\left(\frac{\rho}{\left\|\hat{\boldsymbol{p}}_k - \boldsymbol{p}_k^{i,j}\right\|}\right) & \left\|\hat{\boldsymbol{p}}_k - \boldsymbol{p}_k^{i,j}\right\| > \rho \\ 0 & \left\|\hat{\boldsymbol{p}}_k - \boldsymbol{p}_k^{i,j}\right\| \leq \rho \end{cases} \tag{28}$$

Note that when $\theta_k^{i,j} = 0$ we have $\boldsymbol{r}_k^{i,j} = \boldsymbol{d}_k^{i,j}$ so that the rotated vector $\boldsymbol{r}_k^{i,j}$ can be defined even if $\left\|\hat{\boldsymbol{p}}_k - \boldsymbol{p}_k^{i,j}\right\| \leq \rho$. Lastly, we introduce a rotation factor $\alpha \in [0, 1]$ as a tuning parameter with which we can tune the deflection of the predicted trajectory. The rotated vector is then:

$$\boldsymbol{r}_k^{i,j} = \tilde{\boldsymbol{R}}(\alpha\theta_k^{i,j})\boldsymbol{d}_k^{i,j} \tag{29}$$

The affine constraints will then take the form:

$$\mathcal{H}_r^{i,j} : {\boldsymbol{r}_k^{i,j}}^\top \boldsymbol{p}_k \leq {\boldsymbol{r}_k^{i,j}}^\top \left(\boldsymbol{p}_k^{i,j} + \boldsymbol{r}_k^{i,j}\rho\right) \tag{30}$$

Thus, the red hyperplane of Figure 7 denoted as $\mathcal{H}_r^{i,j}$ reduces smoothly to the orange hyperplane $\mathcal{H}_d^{i,j}$ as $\left\|\hat{\boldsymbol{p}}_k - \boldsymbol{p}_k^{i,j}\right\| \to \rho$ and the constraint can always be defined as long as $\hat{\boldsymbol{p}}_k \neq \boldsymbol{p}_k^{i,j}$. Depending on the traffic role of the ASV we can tune the rotation factor α differently to achieve a deflection of the trajectory as desired. In case the ASV has a GW role, in order to yield trajectories like the first three in Figure 6 this requires $\alpha \to 1$. On the other hand, if the ASV has an EM role, the last two trajectories of Figure 6 will be achieved for $\alpha \to 0$. If the ASV has an SO role, no constraints are imposed and the vessel is required to maintain its course and speed according to Rule 17. Lastly, in order to comply with Rule 8.b that requires readily apparent maneuvers, we can use the current states for the first few meters of the encounter that is, $\hat{\boldsymbol{p}}_k = \boldsymbol{p}_1$ and $\boldsymbol{p}_k^{i,j} = \boldsymbol{p}_1^{i,j}$. This will force a strong alteration of course or speed at the beginning of the encounter so that the actions of the ASV are readily apparent to the OVs.

Since these constraints are computed a priori based on the shifted plan, we can determine which one of them will be active and thus have only one constraint per obstacle to further simplify problem (2). Therefore, there will be a single constraint per OV that is "rolling" along the periphery of the rounded rectangle depending on the relative position and orientation of the ASV and the OV. In summary, each constraint i with $i = 1, \ldots, n$, splits the workspace of the vessels $\mathcal{W}$ in two half-spaces, one containing the i^{th} OV and its counterpart containing the ASV making sure that their footprints are always separated and thus collision avoidance is ensured. Moreover, the deflection tuning of this half-space is used to enforce rule-compliant trajectories. The affine constraints to be inserted in (2) will then take the final form:

$$\mathcal{Z}^R : {\boldsymbol{A}_k^i}^\top \boldsymbol{p}_k \leq b_k^i, \quad i = 1, \ldots, n, \tag{31}$$

with:

$$\boldsymbol{A}_k^i = \boldsymbol{r}_k^{i,j}, \quad b_k^i = {\boldsymbol{A}_k^i}^\top \left(\boldsymbol{p}_k^{i,j} + \boldsymbol{A}_k^i\rho\right), \quad j \in [1, 4] \tag{32}$$

where the index for $j \in [1, 4]$ is chosen so that the corresponding affine constraint does not intersect the inflated rounded rectangle of Figure 7.

Note that the aforementioned considerations regarding i) a well-defined expression of constraints that ensures feasibility and ii) a pre-processing procedure to activate just one constraint per OV were not contemplated in [40]. In addition, in this work, a discussion on the effect of these constraints in traffic situations with multiple OVs follows. The constraint space $\mathcal{Z}^R$ for the position $\boldsymbol{p}$ of the vessel is illustrated qualitatively in Figure 8. The ASV has either a GW or an EM role with respect to each OV and the corresponding affine constraint is generated. When these overlap, they lead to the convex polytope $\mathcal{Z}^R$ which is the search space for the trajectory optimization problem (2). One of the benefits of such a design is that as the ASV and OV move with respect to each other to resolve the traffic situation, the constraints are "rolling" out of the way of the ASV thus not impeding its path anymore. Therefore, they can remain active for as long as the traffic role is active according to Section V without blocking the motion of the ASV. Thus, neither complicated exit criteria nor hysteresis in the decision-making module are needed for the FSM designed in Section V in contrast to other works (e.g., [11, 35]). Note that in Figure 8, the set $\mathcal{Z}^R$ is presented only at the current time. In the optimization problem, there would be N polygons, one for each timestep k along the prediction horizon.

In the context of vessels navigating in dynamic environments with uncertain neighboring agents' intentions, ensuring formal closed-loop stability is challenging. One possible approach to address this issue is by modeling uncertainties in predicting neighboring vehicles' intentions within the motion planning problem and designing a suitable terminal cost in (2a) to ensure stability.

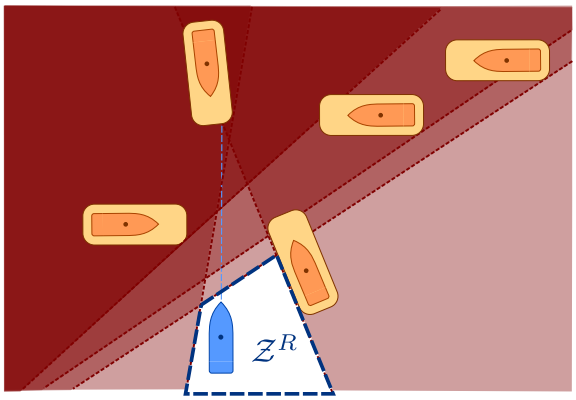

Fig. 8. Multiple half-space constraints active simultaneously that result in a convex search space for the trajectory optimization problem.

Algorithm 1 Traffic role decision making and constraint generation

Input: $\boldsymbol{z}(t)$, $\boldsymbol{z}^i(t), l^i, w^i, \quad \forall i \in [1, \cdots, n]$
Output: $\boldsymbol{A}, \boldsymbol{b}, q_u$ see (31), (32)

for $t = 1, 2, \ldots$ **do**
  for $i \in [1, \cdots, n]$ **do** ▷ Traffic role decision making
    Compute $d(t)$ from Eq. (16)
    Compute $d_{\text{CPA}}(t)$ from Eq. (19)
    Compute $\psi_b^i(t)$ from Eq. (20)
    Compute $\psi_c^i(t)$ from Eq. (21)
    Compute $role^i(t)$ from Eq. (23) and the FSM
  end for
  for $k \in [1, \cdots, N]$ **do** ▷ Constraint generation
    $\hat{\boldsymbol{p}}_k \leftarrow \boldsymbol{p}_{t-1|k+1}, \hat{\boldsymbol{p}}_N \leftarrow 2\boldsymbol{p}_{t-1|N} - \boldsymbol{p}_{t-1|N-1}$
    $\boldsymbol{p}_k^i \leftarrow \boldsymbol{p}^i(t) + k \cdot \Delta k \cdot \tilde{\boldsymbol{R}}(\boldsymbol{z}(t))\boldsymbol{v}^i(t)$
    for $i \in [1, \cdots, n]$ **do**
      if $role^i == SO$ **then**
        $q_u^i \leftarrow q_{u_{\text{SO}}}$
      else
        if $role^i == GW$ **then**
          $q_u^i \leftarrow q_{u_{\text{GW}}}$
          $\alpha \leftarrow [0, 1]$ ▷ Set α value close to 1
        else if $role^i == EM$ **then**
          $q_u^i \leftarrow q_{u_{\text{EM}}}$
          $\alpha \leftarrow [0, 1]$ ▷ Set α value close to 0
        end if
        for $j \in [1, \cdots, 4]$ **do**
          Compute $\boldsymbol{p}_k^{i,j}$ from Eq. (27) given $\boldsymbol{p}_k^i$
          Compute $\boldsymbol{d}_k^{i,j}$ from Eq. (25) given $\hat{\boldsymbol{p}}_k$
          Compute $\theta_k^{i,j}$ from Eq. (28)
          Compute $\boldsymbol{r}_k^{i,j}$ from Eq. (29)
        end for
        Choose $\boldsymbol{r}_k^i$ as the active $\boldsymbol{r}_k^{i,j}$
        Compute $\boldsymbol{A}_k^i, b_k^i$ from Eq. (31)
      end if
    end for
  end for
  $q_u \leftarrow min(q_u^i), \quad \forall i \in [1, \cdots, n]$
  Create $\boldsymbol{A}, \boldsymbol{b}$ by concatenating $\boldsymbol{A}_k^i, b_k^i$
end for

q_{e_l}	q_{e_c}	$q_{u_{\text{EM}}}$	$q_{u_{\text{GW}}}$	q_v	q_{τ_u}	q_{τ_r}
1	10	10	1000	250	0.1	3

TABLE I
OBJECTIVE FUNCTION WEIGHT VALUES

ρ_s	ρ_{enc}	ρ_{emg}	ψ_h	ρ_{bm}^i	ρ_{sn}^i	ρ_{pt}^i	ρ_{sb}^i	α
2	21	10	0.25	l^i	$l^i/2$	w^i	w^i	0.97

TABLE II
GEOMETRY PARAMETER VALUES

VII. SIMULATION RESULTS

This section presents simulation results to validate the efficacy of our algorithm in different traffic scenarios. The first vessel-to-vessel scenarios are chosen to highlight the rule-compliant collision avoidance maneuvers in each possible traffic situation. We then test the algorithm in multi-vessel encounters to show that it does not lead to deadlocks in complex traffic situations and that it is scalable with respect to the number of OVs. Our framework is implemented in ROS: the controller in C++ and the simulator of the ASV and OVs in Python. The solver used relies on the Primal-Dual Interior-Point method and is generated with Forces Pro [52, 53]. The algorithm runs in an Ubuntu machine with an Intel i7 CPU@1.8GHz and 16GB of RAM.

In the following simulation scenarios, the ASV is expected to follow a horizontal reference path along X-axis of the global reference frame at a reference surge velocity $u_{\text{ref}} = 1$m/s while avoiding collisions according to the regulations. The values of the used parameters are summarized in Tables I and II while the numerical values of the ASV model described in (4a) can be found in [54]. For all the OVs the dimensions are the same as the ones used for the ASV: $l^i = l = 1.25$m and $w^i = w = 0.29$m while their longitudinal velocities vary in the range $0.9 - 1.2$m/s. The horizon length is set to $N = 41$ steps and the prediction timestep at $\Delta k = 0.25$s.

Figure 9 demonstrates the ASV's maneuver in an Overtaking situation where the ASV has a GW role. As described in Rule 13, the ASV turns to starboard while it keeps out of the way of the OV. Figure 10 shows the ASV in a Head-On situation and a GW role. In compliance with Rule 14, the ASV changes course to starboard so that each vessel passes on the port side of the other while it keeps out of the way of the OV. Figure 11 illustrates another scenario in which the ASV has a GW role in a Starboard-Crossing situation. In this scenario, the ASV takes a collision avoidance maneuver to its starboard and avoids crossing ahead of the other vessel according to Rule 15. Lastly, Figure 12 presents a Port-Crossing situation where the ASV normally would have an SO role, but the OV does not comply with the rules and does not take action to avoid collision. In this case, the ASV has an EM role and needs to take action to avoid collision while it does not alter its course to port for a vessel on its own port side. Notice that in every scenario, the ASV autonomously performs maneuvers that are clear and readily apparent thus complying with Rule 8.

A multi-vessel encounter is illustrated in Figure 13 where the ASV is able to successfully avoid collision with each vessel obstacle in a rule-compliant manner. The ASV first

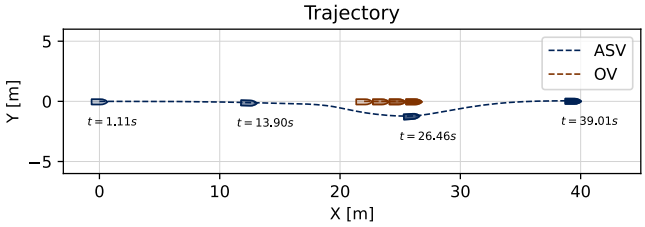

Fig. 9. Overtaking situation with the ASV in GW role, turning to starboard while it keeps out of the way of the OV (Rule 13.)

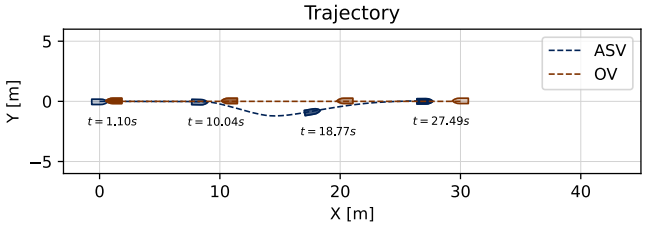

Fig. 10. Head-On situation with the ASV in GW role, turning to starboard so that each vessel passes on the other's port (Rule 14).

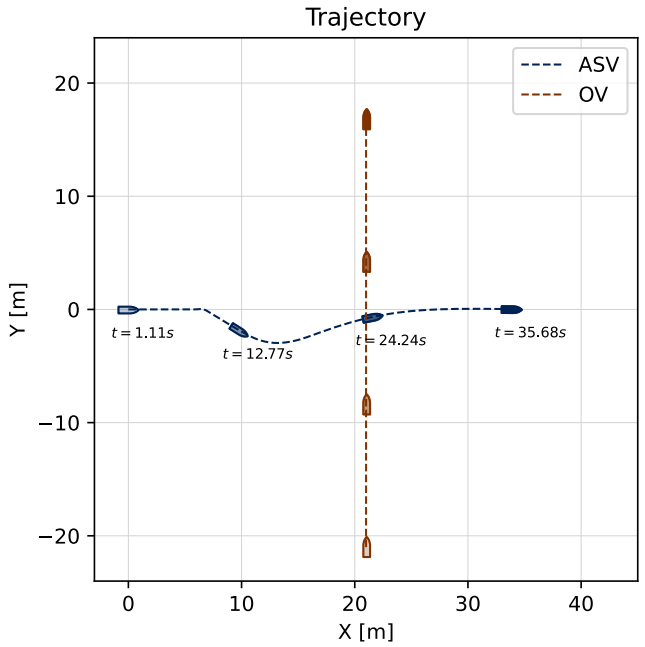

Fig. 11. Starboard Crossing situation with the ASV in GW role, turning to starboard while avoiding crossing ahead of the other vessel (Rule 15).

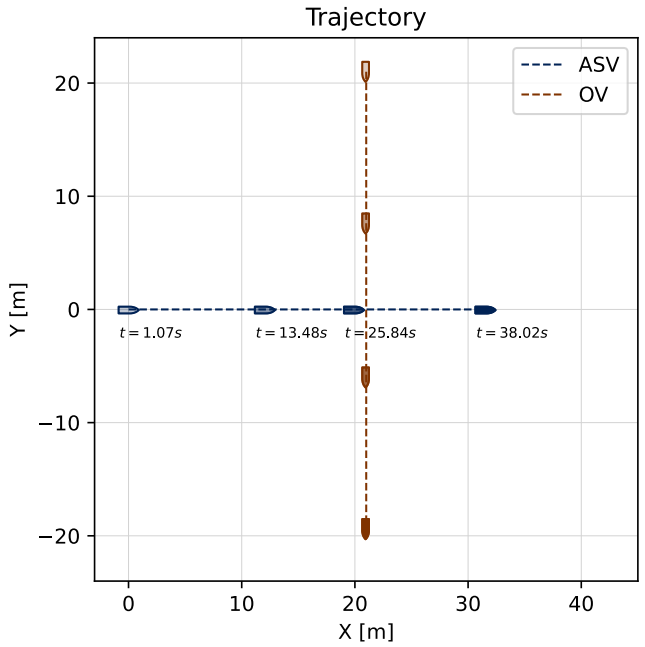

Fig. 12. Port Crossing situation with the ASV in EM role, passing behind the non-compliant vessel (Rule 17).

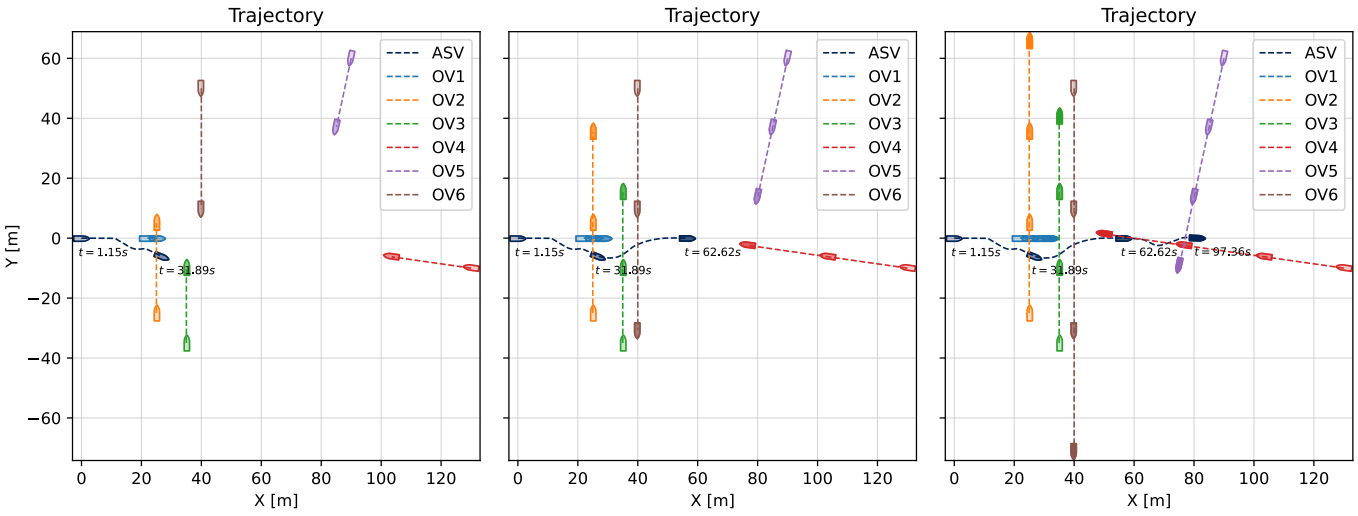

Fig. 13. Trajectories in a multi-vessel encounter situation with the ASV passing through multiple OVs while following a horizontal path.

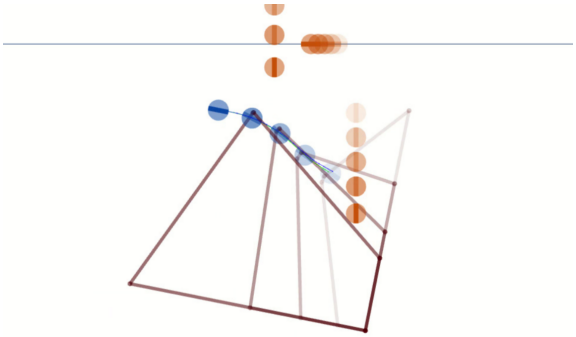

Fig. 14. A screenshot from RVIZ to illustrate the convex polytope constraints generated along the prediction horizon for timestep $k = 10, 20, 30, 40$.

encounters OV 1 and attempts to overtake it. A bit later it encounters two vessels (OV 2 and 3) crossing from its starboard side so it alters course to starboard to pass behind them. As soon as it returns to its reference path, OV 6 is coming from its port side not complying with the rules, and thus the ASV reduces speed to avoid collision. Right after, the ASV encounters OV 4 in a head-on situation and OV 5 in a port-crossing situation. At first, it changes course to starboard and later slows down to successfully avoid collision with both, according to the rules. The simulation environment in which we run our experiments (RVIZ) is illustrated in Figure 14 where the constraint polytopes can be seen along the prediction horizon. The corresponding state and input of the system for the multi-vessel scenario is provided in Figures 15, 16, and 17. In Figure 18 the successive traffic roles are shown as the ASV navigates through traffic. The ASV has a GW role with respect to OV 1, 2, 3 and 4 and an SO role with respect to OV 5 and 6. The latter do not comply with the rules and thus an EM role emerges for the ASV as they approach in dangerous proximity. In Figure 19 we compare the relative distance between the ASV and each OV i to the minimum accepted distance for collision avoidance ($\rho+\rho^i$). Note that this is more conservative than what we enforce with the collision avoidance constraints, but it is used just as an indication that collision avoidance is achieved. Lastly, we show in Figure 20 the computation time with respect to the increasing number of obstacles to illustrate the scalability of the algorithm. The average time for the control loop is on average about 33 ms for every run showing that the number of obstacles does not complicate the solution of the optimization problem.

VIII. Conclusions & Future Work

In this work, we proposed a trajectory optimization and control algorithm for safe navigation of ASVs in mixed-traffic environments by incorporating COLREGs as constraints. The efficacy of the proposed algorithm was validated via different simulation scenarios involving relevant rule-compliant collision avoidance maneuvers that comply with COLREGs. Scenarios with multiple vessels were also tested to show the algorithm's ability to handle complex traffic situations without deadlocks and its scalability with respect to the number of obstacles. For future work, we aim to robustify the algorithm against uncertainties and faults.

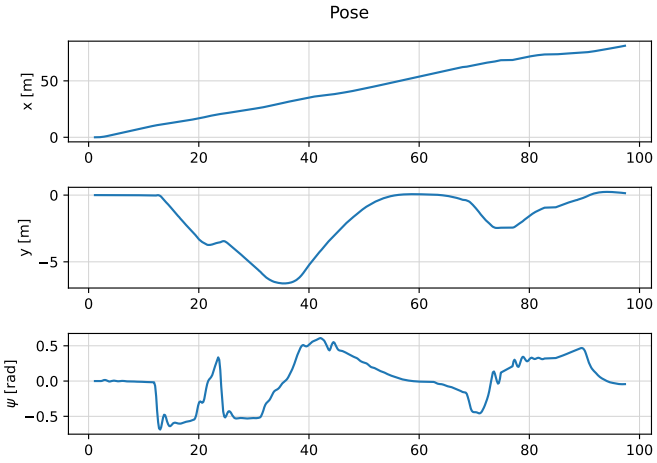

Fig. 15. Pose (position and orientation) of the ASV for the multi-vessel encounter presented in Figure 13.

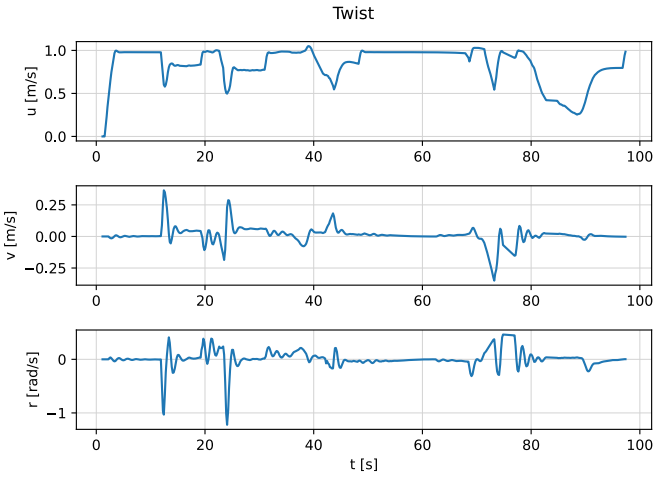

Fig. 16. Twist (translational and rotational velocities) of the ASV for the multi-vessel encounter presented in Figure13.

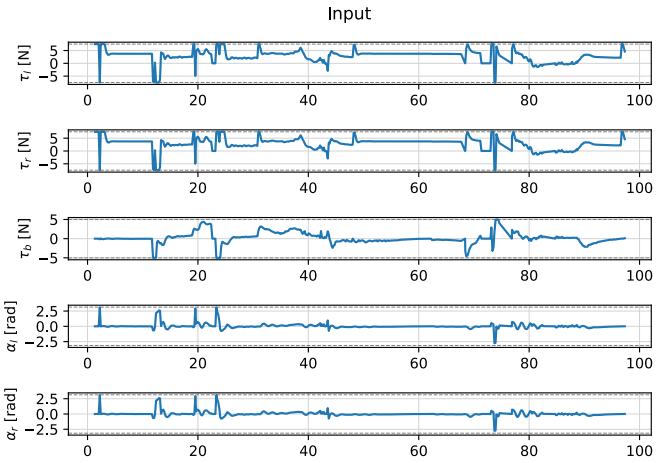

Fig. 17. Control input of the ASV for the multi-vessel encounter presented in Figure 13.

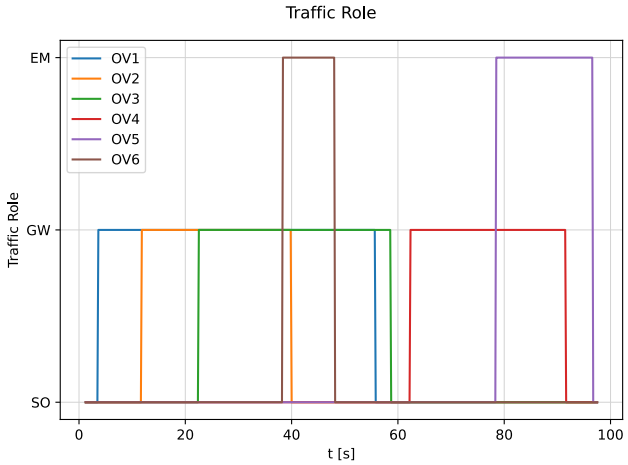

Fig. 18. Traffic role for the ASV with respect to each OV corresponding to the traffic situations that emerge in Figure 13.

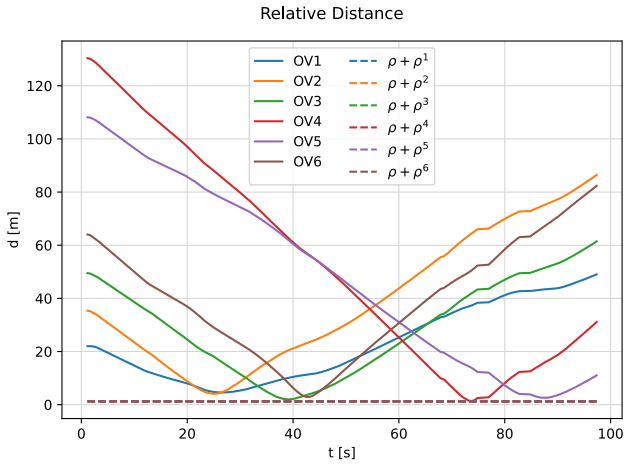

Fig. 19. The distance between the ASV and each OV in the scenario presented in Figure 13 as a function of time. The lower dashed line represents the sum of $\rho + \rho^i$ for each OV showing that there is no collision.

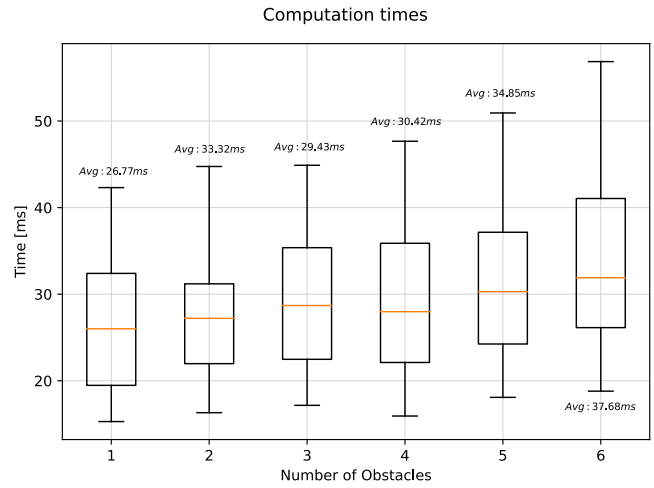

Fig. 20. Computation times for increasing number of obstacles: The average computation time remains similar meaning that the additional constraints do not complicate the solution of the optimization problem.

REFERENCES

[1] Y. Gu, J. C. Goez, M. Guajardo, and S. W. Wallace, "Autonomous vessels: State of the art and potential opportunities in logistics," *International Transactions in Operational Research*, vol. 28, no. 4, pp. 1706–1739, 2021.

[2] I. Berman *et al.*, "Trustable environmental monitoring by means of sensors networks on swarming autonomous marine vessels and distributed ledger technology," *Frontiers in Robotics and AI*, vol. 7, 2020.

[3] A. Matos *et al.*, "Unmanned maritime systems for search and rescue," *Search and Rescue Robotics-From Theory to Practice*, pp. 77–92, 2017.

[4] EMSA, *Annual Overview of Marine Casualties and Incidents*, http://www.emsa.europa.eu, 2021.

[5] Y. Huang, L. Chen, P. Chen, R. R. Negenborn, and P. van Gelder, "Ship collision avoidance methods," *Safety Science*, vol. 121, pp. 451–473, 2020.

[6] "COLREGs - International Regulations for Preventing Collisions at Sea," *Convention on the International Regulations for Preventing Collisions at Sea, 1972*, pp. 1–74, 1972.

[7] A. Bakdi and E. Vanem, "Fullest COLREGs evaluation using fuzzy logic for collaborative decision-making analysis of autonomous ships in complex situations," *IEEE Transactions on Intelligent Transportation Systems*, vol. 23, no. 10, pp. 18 433–18 445, 2022.

[8] Y. Cho, J. Han, and J. Kim, "Intent inference of ship maneuvering for automatic ship collision avoidance," *IFAC-PapersOnLine*, vol. 51, no. 29, pp. 384–388, 2018.

[9] S. V. Rothmund, T. Tengesdal, E. F. Brekke, and T. A. Johansen, "Intention modeling and inference for autonomous collision avoidance at sea," *Ocean Engineering*, vol. 266, p. 113 080, 2022.

[10] P. N. Hansen *et al.*, "COLREGs-based situation awareness for marine vessels-a discrete event systems approach," *IFAC-PapersOnLine*, vol. 53, no. 2, pp. 14 501–14 508, 2020.

[11] Y. Kuwata, M. T. Wolf, D. Zarzhitsky, and T. L. Huntsberger, "Safe maritime autonomous navigation with COLREGs, using velocity obstacles," *IEEE Journal of Oceanic Engineering*, vol. 39, no. 1, pp. 110–119, 2013.

[12] E. H. Thyri and M. Breivik, "Partly COLREGs-compliant collision avoidance for asvs using encounter-specific velocity obstacles," *IFAC-PapersOnLine*, vol. 55, no. 31, pp. 37–43, 2022.

[13] Y. Huang, L. Chen, and P. van Gelder, "Generalized velocity obstacle algorithm for preventing ship collisions at sea," *Ocean Engineering*, vol. 173, pp. 142–156, 2019.

[14] Y. Cho, J. Han, and J. Kim, "Efficient COLREGs-Compliant Collision Avoidance in Multi-Ship Encounter Situations," *IEEE Transactions on Intelligent Transportation Systems*, vol. 23, no. 3, pp. 1899–1911, 2020.

[15] D. K. Kufoalor, E. F. Brekke, and T. A. Johansen, "Proactive collision avoidance for ASVs using a

dynamic reciprocal velocity obstacles method," in *2018 IEEE/RSJ International Conference on Intelligent Robots and Systems (IROS)*, 2018, pp. 2402–2409.

[16] Y. Zhao, W. Li, and P. Shi, "A real-time collision avoidance learning system for Unmanned Surface Vessels," *Neurocomputing*, vol. 182, pp. 255–266, 2016.

[17] Y. Xue, B. Lee, and D. Han, "Automatic collision avoidance of ships," *Proceedings of the Institution of Mechanical Engineers, Part M: Journal of Engineering for the Maritime Environment*, vol. 223, no. 1, pp. 33–46, 2009.

[18] W. Naeem, S. C. Henrique, and L. Hu, "A Reactive COLREGs-Compliant Navigation Strategy for Autonomous Maritime Navigation," *IFAC-PapersOnLine*, vol. 49, no. 23, pp. 207–213, 2016.

[19] H. Lyu and Y. Yin, "COLREGs-Constrained Real-Time Path Planning for Autonomous Ships Using Modified Artificial Potential Fields," *Journal of Navigation*, vol. 72, no. 3, pp. 588–608, 2019.

[20] P. Švec, A. Thakur, E. Raboin, B. C. Shah, and S. K. Gupta, "Target following with motion prediction for unmanned surface vehicle operating in cluttered environments," *Autonomous Robots*, vol. 36, no. 4, pp. 383–405, 2014.

[21] P. Agrawal and J. M. Dolan, "COLREGs-compliant target following for an Unmanned Surface Vehicle in dynamic environments," in *2015 IEEE/RSJ International Conference on Intelligent Robots and Systems (IROS)*, 2015, pp. 1065–1070.

[22] Z. He, C. Liu, X. Chu, R. R. Negenborn, and Q. Wu, "Dynamic anti-collision A-star algorithm for multi-ship encounter situations," *Applied Ocean Research*, vol. 118, p. 102 995, 2022.

[23] M. Candeloro, A. M. Lekkas, and A. J. Sørensen, "A voronoi-diagram-based dynamic path-planning system for underactuated marine vessels," *Controlunder Engineering Practice*, vol. 61, pp. 41–54, 2017.

[24] H. T. L. Chiang and L. Tapia, "COLREGs-RRT: An RRT-Based COLREGs-Compliant Motion Planner for Surface Vehicle Navigation," *IEEE Robotics and Automation Letters*, vol. 3, no. 3, pp. 2024–2031, 2018.

[25] T. T. Enevoldsen, C. Reinartz, and R. Galeazzi, "COLREGs-informed RRT* for collision avoidance of marine crafts," in *2021 IEEE International Conference on Robotics and Automation (ICRA)*, 2021, pp. 8083–8089.

[26] E. Meyer, A. Heiberg, A. Rasheed, and O. San, "COLREGs-compliant collision avoidance for unmanned surface vehicle using deep reinforcement learning," *IEEE Access*, vol. 8, pp. 165 344–165 364, 2020.

[27] X. Xu, Y. Lu, X. Liu, and W. Zhang, "Intelligent collision avoidance algorithms for USVs via deep reinforcement learning under COLREGs," *Ocean Engineering*, vol. 217, p. 107 704, 2020.

[28] T. A. Johansen, T. Perez, and A. Cristofaro, "Ship Collision Avoidance and COLREGs Compliance Using Simulation-Based Control Behavior Selection With Predictive Hazard Assessment," *IEEE Transactions on Intelligent Transportation Systems*, vol. 17, no. 12, pp. 3407–3422, 2016.

[29] I. B. Hagen, D. K. M. Kufoalor, E. F. Brekke, and T. A. Johansen, "MPC-based collision avoidance strategy for existing marine vessel guidance systems," in *2018 IEEE ICRA*, IEEE, 2018, pp. 7618–7623.

[30] D. K. Kufoalor, E. Wilthil, I. B. Hagen, E. F. Brekke, and T. A. Johansen, "Autonomous COLREGs-compliant decision making using maritime radar tracking and model predictive control," *18th European Control Conference*, pp. 2536–2542, 2019.

[31] T. Tengesdal, T. A. Johansen, and E. F. Brekke, "Ship collision avoidance utilizing the cross-entropy method for collision risk assessment," *IEEE Transactions on Intelligent Transportation Systems*, vol. 23, no. 8, pp. 11 148–11 161, 2021.

[32] I. Hagen, D. Kufoalor, T. Johansen, and E. Brekke, "Scenario-based model predictive control with several steps for COLREGs compliant ship collision avoidance," *IFAC-PapersOnLine*, vol. 55, no. 31, pp. 307–312, 2022.

[33] L. Hu *et al.*, "A multiobjective optimization approach for COLREGs-compliant path planning of autonomous surface vehicles verified on networked bridge simulators," *IEEE Transactions on Intelligent Transportation Systems*, vol. 21, no. 3, pp. 1167–1179, 2019.

[34] M. Abdelaal, M. Fränzle, and A. Hahn, "Nonlinear Model Predictive Control for trajectory tracking and collision avoidance of underactuated vessels with disturbances," *Ocean Engineering*, vol. 160, pp. 168–180, 2018.

[35] B.-O. H. Eriksen, G. Bitar, M. Breivik, and A. M. Lekkas, "Hybrid Collision Avoidance for ASVs Compliant With COLREGs Rules 8 and 13–17," *Frontiers in Robotics and AI*, vol. 7, 2020.

[36] Z. Du, R. R. Negenborn, and V. Reppa, "Multi-objective cooperative control for a ship-towing system in congested water traffic environments," *IEEE Transactions on Intelligent Transportation Systems*, vol. 23, no. 12, pp. 24 318–24 329, 2022.

[37] J. de Vries, E. Trevisan, J. van der Toorn, T. Das, B. Brito, and J. Alonso-Mora, "Regulations aware motion planning for autonomous surface vessels in urban canals," in *2022 International Conference on Robotics and Automation (ICRA)*, 2022, pp. 3291–3297.

[38] M. Abdelaal and A. Hahn, "Nmpc-based trajectory tracking and collision avoidance of unmanned surface vessels with rule-based COLREGs confinement," in *2016 IEEE Conference on Systems, Process and Control (ICSPC)*, IEEE, 2016, pp. 23–28.

[39] E. H. Thyri and M. Breivik, "Collision avoidance for ASVs through trajectory planning: MPC with COLREGs-compliant nonlinear constraints," *Modeling, Identification and Control*, vol. 43, no. 2, pp. 55–77, 2022.

[40] A. Tsolakis, D. Benders, O. de Groot, R. R. Negenborn, V. Reppa, and L. Ferranti, "COLREGs-aware Trajectory Optimization for Autonomous Surface Vessels," *IFAC-*

PapersOnLine, vol. 55, no. 31, pp. 269–274, 2022, 14th IFAC Conference on Control Applications in Marine Systems, Robotics, and Vehicles CAMS 2022.

[41] W. Schwarting, J. Alonso-Mora, L. Paull, S. Karaman, and D. Rus, "Safe nonlinear trajectory generation for parallel autonomy with a dynamic vehicle model," *IEEE Transactions on Intelligent Transportation Systems*, vol. 19, no. 9, pp. 2994–3008, Sep. 2018.

[42] L. Ferranti, L. Lyons, R. R. Negenborn, T. Keviczky, and J. Alonso-Mora, "Distributed nonlinear trajectory optimization for multi-robot motion planning," *IEEE Transactions on Control Systems Technology*, 2022.

[43] B. Brito, B. Floor, L. Ferranti, and J. Alonso-Mora, "Model Predictive Contouring Control for Collision Avoidance in Unstructured Dynamic Environments," *IEEE Robotics and Automation Letters*, vol. 4, no. 4, pp. 4459–4466, 2019.

[44] O. de Groot, B. Brito, L. Ferranti, D. Gavrila, and J. Alonso-Mora, "Scenario-Based Trajectory Optimization in Uncertain Dynamic Environments," *IEEE Robotics and Automation Letters*, vol. 6, no. 3, pp. 5389–5396, 2021.

[45] O. de Groot, L. Ferranti, D. Gavrila, and J. Alonso–Mora, "Globally guided trajectory planning in dynamic environments," in *2023 IEEE International Conference on Robotics and Automation (ICRA)*, IEEE, 2023, pp. 10 118–10 124.

[46] D. Qiao, G. Liu, T. Lv, W. Li, and J. Zhang, "Marine Vision-Based Situational Awareness Using Discriminative Deep Learning: A Survey," *Journal of Marine Science and Engineering*, vol. 9, no. 4, 2021.

[47] V. Garofano, M. Hepworth, and R. Shahin, "Obstacle Avoidance and Trajectory Optimization for an Autonomous Vessel Utilizing MILP Path Planning, Computer Vision based Perception and Feedback Control," in *Proceedings of the International Ship Control Systems Symposium*, vol. 16, 2022, p. 11.

[48] T. I. Fossen, *Handbook of Marine Craft Hydrodynamics and Motion Control*. John Wiley & Sons, 2011.

[49] L. Du, O. A. V. Banda, F. Goerlandt, Y. Huang, and P. Kujala, "A COLREGs-compliant ship collision alert system for stand-on vessels," *Ocean Engineering*, vol. 218, p. 107 866, 2020.

[50] F. Borrelli, A. Bemporad, and M. Morari, *Predictive control for linear and hybrid systems*. Cambridge University Press, 2017.

[51] S. Boyd, S. P. Boyd, and L. Vandenberghe, *Convex optimization*. Cambridge university press, 2004.

[52] A. Domahidi and J. Jerez, *FORCES Professional*, Embotech AG, 2023.

[53] A. Zanelli, A. Domahidi, J. Jerez, and M. Morari, "FORCES NLP," *International Journal of Control*, pp. 1–17, 2017.

[54] R. Skjetne, Ø. Smogeli, and T. I. Fossen, "Modeling, identification, and adaptive maneuvering of CyberShip II: A complete design with experiments," *IFAC Proceedings Volumes*, vol. 37, no. 10, pp. 203–208, 2004, IFAC Conference on Computer Applications in Marine Systems - CAMS 2004, Ancona, Italy, 7-9 July 2004.

Anastasios Tsolakis received the diploma in Mechanical Engineering from Aristotle University of Thessaloniki (AUTH), Greece in 2018. In 2021 he received the M.Sc degree in Systems & Control from Delft University of Technology, Delft, The Netherlands. He is currently pursuing the Ph.D. degree with the department of Cognitive Robotics, at Delft University of Technology. His research focuses on the cooperation of autonomous vehicles in mixed-traffic environments.

Rudy R. Negenborn is a Full Professor in "Multi-Machine Operations & Logistics" at Delft University of Technology. He is head of the Section Transport Engineering & Logistics at the Department of Maritime & Transport Technology, and leads the Researchlab Autonomous Shipping (RAS). His research interests include automatic control and coordination of transport technology, with a focus on smart shipping and smart logistics applications. He has over 300 peer reviewed publications and leads NWO, EU and industry funded research, such as the Horizon 2020 program NOVIMOVE.

Vasso Reppa (Member, IEEE) has been an Assistant Professor with the Department of Maritime and Transport Technology, Delft University of Technology, The Netherlands, since 2018. She received the Ph.D. degree in electrical and computer engineering from the University of Patras, Greece, in 2010. From 2011 to 2017, she was a Research Associate (now Research Affiliate) with the KIOS Research and Innovation Center of Excellence, Cyprus. In 2013, she was awarded the Marie Curie Intra European Fellowship and worked as a Research Fellow with CentraleSupélec, University of Paris-Saclay, France, from 2014 to 2016. She was a Visiting Researcher with Imperial College London, U.K., in 2015; and with The University of Newcastle, Australia, in 2016. Her current research interests include multi-agent fault diagnosis and fault tolerant control, cooperative control, adaptive learning, observer-based estimation, and applications of autonomous maritime transport and smart buildings. She has been involved in several research and development projects (e.g., HorizonEurope "SEAMLESS", H2020 "NOVIMOVE, " NWO "READINESS," and Marie Curie ETN "AUTOBarge").

Laura Ferranti received the Ph.D. degree from the Delft University of Technology, Delft, The Netherlands, in 2017. She is currently an Assistant Professor with the Cognitive Robotics (CoR) Department, Delft University of Technology. Her research interests include optimization and optimal control, model predictive control, reinforcement learning, embedded optimization-based control with application in flight control, maritime transportation, robotics, and automotive. Dr. Ferranti was a recipient of the NWO Veni Grant from the Netherlands Organization for Scientific research in 2020 and the Best Paper Award on Multi-Robot Systems at International Conference on robotics and Automation (ICRA) 2019.